

Invasiveness of nonequilibrium pure-dephasing quantum thermometryFrancesco Albarelli ^{*}, Matteo G. A. Paris , Bassano Vacchini , and Andrea Smirne *Dipartimento di Fisica “Aldo Pontremoli,” Università degli Studi di Milano, via Celoria 16, 20133 Milan, Italy
and Istituto Nazionale di Fisica Nucleare, Sezione di Milano, via Celoria 16, 20133 Milan, Italy*

(Received 15 May 2023; revised 25 November 2023; accepted 29 November 2023; published 21 December 2023)

One of the main advantages expected from using quantum probes as thermometers is noninvasiveness, i.e., a negligible perturbation to the thermal sample. However, invasiveness is rarely investigated explicitly. Here, focusing on a spin probe undergoing pure dephasing due to the interaction with a bosonic sample, we show that there is a nontrivial relation between the information on the temperature gained by a quantum probe and the heat absorbed by the sample due to the interaction. We show that time-optimal probing schemes obtained by considering the total experiment time as a resource also have the benefit of limiting the heat absorbed by the sample in each shot of the experiment. For such time-optimal protocols, we show that it is advantageous to have strong probe-sample coupling, since in this regime the accuracy increases linearly with the coupling strength, while the amount of heat per shot saturates to a finite value. Since in pure-dephasing models the absorbed heat corresponds to the external work needed to couple and decouple the probe and the sample, our results also represent a first step towards the analysis of the thermodynamic and energetic cost of quantum thermometry.

DOI: [10.1103/PhysRevA.108.062421](https://doi.org/10.1103/PhysRevA.108.062421)**I. INTRODUCTION**

Estimating the temperature of a quantum system is a task of fundamental and practical importance. Many quantum technologies require very low temperatures to exploit fragile nonclassical features; thus temperature must be assessed with great accuracy while disturbing the system as little as possible. This is the goal of quantum thermometry, a fertile research field at the intersection of quantum metrology, quantum thermodynamics, and open quantum systems [1,2]. The accuracy of equilibrium quantum thermometry has been extensively discussed [3–7]. Going beyond equilibrium, temperature can be estimated via quantum probes interacting with a thermal sample, modeling the probe as an open quantum system [8] and the sample as a bosonic [3,9–14] or fermionic [15–17] environment, or by means of collisional approaches [18–21]. Open quantum systems may also be used to probe other environmental parameters [22–25] and for quantum noise spectroscopy [26–28]. In recent experiments, impurities in quantum gases have been used as thermometric probes [29–31].

In this paper we investigate the perturbation induced on the initial thermal state of the sample by the interaction with the probe. We will call *invasiveness* this feature of nonequilibrium thermometry protocols.¹ Crucially, quantifying invasiveness also requires a study of the dynamics of the environment [32–39], especially important also in strong-coupling quantum thermodynamics [40–42].

Concretely, we propose to quantify the invasiveness of probe-based thermometric protocols in terms of the average heat absorbed by the sample, a choice informed by thermodynamics. We consider the spin-boson model [43], where an environment of harmonic oscillators constitutes a thermal sample coupled to a spin probe. We focus on a coupling that preserves the probe’s internal energy, inducing a pure-dephasing dynamics that can be exploited for thermometry [12,28,44–46]. Since the probe does not exchange energy with the environment, the thermodynamic features of the model may appear trivial. However, external work is needed to couple and decouple the probe and the sample, and heat is dissipated into the environment [47–49], perturbing the sample from its initial state of thermal equilibrium.

The manuscript is structured as follows. In Sec. II we introduce the model, i.e., the pure-dephasing interaction between the probe and the sample, the relevant figures of merit, and their expressions. Section III contains explicit results showing the interplay between thermometric accuracy and invasiveness for a two-level probe coupled to a sample with an Ohmic-like spectral density with exponential cutoff. Section IV concludes the paper with some remarks and outlooks.

II. MODEL AND FIGURES OF MERIT

In this section we present the general pure-dephasing model, define the relevant figures of merit, and present explicit formulas for a specific instance that will be the basis for the results presented in Sec. III. We highlight here the most important equations derived in this section, so that the reader who is already familiar with these topics may skip the derivations and go straight to Sec. III. The unitary evolution operator of the joint probe and sample system is in Eqs. (2) and (3), the dephasing function is in Eq. (9), and the heat absorbed by

^{*}francesco.albarelli@gmail.com¹To avoid confusion, we stress that this is not the notion of invasiveness appearing in the context of Leggett-Garg inequalities (which has also been connected to quantum metrology [88]).

the sample in Eq. (13). Specific results for two-level probes coupled to a sample with a Ohmic-like spectral density with exponential cutoff are presented in Sec. II C and form the basis of the results shown in Sec. III. In particular, the explicit form of the dephasing function is in Eq. (15), which can be used to evaluate the thermometric accuracy in terms of the quantum Fisher information (QFI) in Eq. (18), while the absorbed heat is reported in Eq. (16).

A. Dephasing dynamics of the probe

We consider a finite-dimensional probe system with a generic Hamiltonian $H_S = \sum_j \epsilon_j |j\rangle\langle j|$, where $|j\rangle$ is the energy eigenbasis. The environment, i.e., the sample (we will use the terms interchangeably), is modeled as noninteracting harmonic oscillators with free Hamiltonian $H_E = \sum_k \omega_k b_k^\dagger b_k$, described by bosonic operators $[b_j, b_k^\dagger] = \delta_{jk}$. The system and environment are coupled by the interaction Hamiltonian $H_I = A_S \otimes (\sum_k f_k b_k^\dagger + f_k^* b_k)$, with $A_S = \sum_j g_j |j\rangle\langle j|$ diagonal in the energy eigenbasis. The joint system-environment state evolves unitarily as $\rho_{SE}(t) = U(t)\rho_{SE}(0)U(t)^\dagger$, with $U(t) = \exp[-it(H_S + H_I + H_E)]$. Since $[H_S, A_S] = 0$, the system undergoes a pure-dephasing dynamics: the populations of the energy levels are constants of motion, while the off-diagonal elements of the reduced density matrix $\rho_S(t) = \text{Tr}_E[\rho_{SE}(t)]$ in the energy eigenbasis evolve as $\rho_S(t) = \sum_{ij} \rho_{S,ij}(0) e^{-i\Delta_{ij}(t) + i\varphi_{ij}(t)} |i\rangle\langle j|$, with real dephasing functions $\Delta_{ij}(t)$ and phases $\varphi_{ij}(t)$. We will now derive explicit expressions for $U(t)$ and for these functions.

1. Global system-environment unitary evolution operator

Going to the interaction picture we obtain the time-dependent Hamiltonian

$$H_I(t) = \sum_j g_j |j\rangle\langle j| \otimes \left(\sum_k f_k e^{i\omega_k t} b_k^\dagger + f_k^* e^{-i\omega_k t} b_k \right), \quad (1)$$

that satisfies $[H_I(t), H_I(t')] = -2i \sum_{j,k} g_j^2 |f_k|^2 \sin \omega_k(t-t') |j\rangle\langle j| \otimes \mathbb{1}$ and thus the time-ordered exponential $U_I(t) = \mathcal{T}_{\leftarrow} \exp^{-i \int_0^t ds H_I(s)}$ can be obtained exactly, e.g., via the Magnus expansion which terminates at second order:

$$\begin{aligned} U_I(t) &= \exp \left[-\frac{1}{2} \int_0^t ds \int_0^s ds' [H_I(s), H_I(s')] \right] \\ &\quad \times \exp \left[-i \int_0^t ds H_I(s) \right] \\ &= \sum_j e^{i\phi_j^{\text{int}}(t)} |j\rangle\langle j| \otimes \prod_k D(\alpha_k^j(t)), \end{aligned} \quad (2)$$

where we have defined $\phi_j^{\text{int}}(t) \equiv \sum_k |f_k|^2 g_j^2 \frac{\omega_k t - \sin(\omega_k t)}{\omega_k^2}$, and the action on the oscillators is a product of single-mode displacements $D(\alpha) = \exp[\alpha b^\dagger - \alpha^* b]$ with

$$\alpha_k^j(t) = -i f_k g_j \int_0^t ds e^{i\omega_k s} = f_k g_j \frac{1 - e^{i\omega_k t}}{\omega_k}. \quad (3)$$

Thus the overall evolution amounts to a displacement of the oscillators conditioned on the state of the system.

2. Reduced state of the system

We write a generic initial state in block form as $\rho_{SE}(0) = \sum_{ij} \rho_{S,ij}(0) |i\rangle\langle j| \otimes \rho_E^{ij}$, where $\text{Tr}_E \rho_E^{ij} = 1$ are normalized operators, but not necessarily positive semidefinite when $i \neq j$. When $i = j$ these are the conditional states obtained with probability $\rho_{S,ii}(0)$ by measuring the system in the basis $|j\rangle$. This means that the initial reduced state of the system is $\rho_S(0) = \text{Tr}_E \rho_{SE}(0) = \sum_{ij} \rho_{S,ij}(0) |i\rangle\langle j|$. We can thus write the evolved state as

$$\begin{aligned} \rho_S(t) &= \sum_{i \neq j} \rho_{S,ii}(0) |i\rangle\langle i| + \sum_{i \neq j} \rho_{S,ij}(0) e^{i(\phi_i^{\text{int}}(t) - \phi_j^{\text{int}}(t))} \\ &\quad \times \text{Tr}_E \left[\prod_k D(\alpha_k^i(t)) \rho_E^{ij} \prod_{k'} D(-\alpha_{k'}^j(t)) \right] |i\rangle\langle j|, \end{aligned} \quad (4)$$

showing explicitly that the populations are constants of motion, since $\text{Tr}_E [\prod_k D(\alpha_k^i(t)) \rho_E^{ii} \prod_{k'} D(-\alpha_{k'}^i(t))] = 1$. Note that (4) includes the possibility of having initial system-environment correlations—see also [50] for a study of pure dephasing with correlated initial states.

We further assume an initial factorized state $\rho_{SE}(0) = \rho_S(0) \otimes \rho_E(0)$ and an initial Gibbs thermal state $\rho_E(0) = e^{-\frac{H_E}{T}} / Z_T$ of the environment, where $Z_T = \text{Tr}[e^{-\frac{H_E}{T}}]$ is the partition function. We choose units such that $\hbar = 1$ and $\kappa_B = 1$, i.e., both temperature and energy are measured as frequencies. The thermal state of the environment is factorized into thermal states of each mode $\nu_k = e^{-\frac{\omega_k}{T} b_k^\dagger b_k} / \text{Tr}[e^{-\frac{\omega_k}{T} b_k^\dagger b_k}]$, since the oscillators are not interacting. The evolved global state in the interaction picture is

$$\begin{aligned} \rho_{SE}(t) &= U_I(t)(\rho_S(0) \otimes \rho_E(0))U_I(t)^\dagger \\ &= \sum_{ij} \rho_{S,ij}(0) e^{i(\phi_i^{\text{int}}(t) - \phi_j^{\text{int}}(t))} |i\rangle\langle j| \\ &\quad \otimes \prod_k D(\alpha_k^i(t)) \rho_E(0) D(-\alpha_k^j(t)). \end{aligned} \quad (5)$$

To evaluate the trace on the environment we use the Baker-Campbell-Hausdorff formula to obtain

$$\begin{aligned} \text{Tr}_k [D(\alpha_k^i(t)) \nu_k D(-\alpha_k^j(t))] \\ = \text{Tr}_k [D(\alpha_k^i(t) - \alpha_k^j(t)) \nu_k] e^{\frac{1}{2}(-\alpha_k^i(t)\alpha_k^{*j}(t) + \alpha_k^{*i}(t)\alpha_k^j(t))}, \end{aligned} \quad (6)$$

where now $\text{Tr}_k [D(\alpha) \nu_k] = \exp[-\frac{1}{2} |\alpha|^2 \coth(\frac{\omega_k}{2T})]$ is the characteristic function of a thermal state.

Keeping track of the phase factors, the reduced system state $\rho_S(t) = \text{Tr}_E [\rho_{SE}(t)]$ in the Schrödinger picture is thus

$$\rho_S(t) = \sum_{ij} \rho_{S,ij}(0) e^{-(\Delta_{ij}(t) + i\varphi_{ij}(t))} |i\rangle\langle j|, \quad (7)$$

where the real-valued dephasing function affecting the off-diagonal elements is

$$\begin{aligned} \Delta_{ij}(t) &= - \sum_k \ln \text{Tr}_k [D(\alpha_k^i(t) - \alpha_k^j(t)) \nu_k] \\ &= \sum_k \frac{1}{2} |\alpha_k^i(t) - \alpha_k^j(t)|^2 \coth\left(\frac{\omega_k}{2T}\right), \end{aligned} \quad (8)$$

and the phase factor includes the usual difference of unitary phases $\phi_j^{\text{Sch}}(t) = \phi_j^{\text{int}}(t) - t\epsilon_j$, containing both the effect of the system Hamiltonian and the phases appearing in the interaction-picture unitary (2), so that the phases in (7) are $\varphi_{ij}(t) = \phi_j^{\text{Sch}}(t) - \phi_i^{\text{Sch}}(t)$. Besides being obviously irrelevant for energetic considerations, the phase factors do not depend on the environment initial state and thus on the temperature, so they are also irrelevant for thermometry and we will neglect them (formally, working in a suitable rotating frame). However, they may be useful to learn properties of the environment spectral density, see, e.g., Ref. [28].

Taking the continuous limit, informally $\sum_k |f_k|^2 \mapsto \int_0^\infty d\omega J(\omega)$, where $J(\omega)$ is the spectral density that includes both the density of states of the sample and a nonuniform distribution of the coupling parameters f_k , and using the definition (3) we obtain the temperature-dependent dephasing functions $\Delta_{ij}(t) = (g_i - g_j)^2 \Delta_T(t)$, where

$$\Delta_T(t) = \int_0^\infty d\omega J(\omega) \frac{1 - \cos \omega t}{\omega^2} \coth\left(\frac{\omega}{2T}\right). \quad (9)$$

B. Heat absorbed by the sample

We define the average heat absorbed by the sample as the variation of the expectation value of its Hamiltonian [41] $Q(t) = \text{Tr}_E H_E[\rho_E(t) - \rho_E(0)]$, with $\rho_E(t) = \text{Tr}_S \rho_{SE}(t)$. Even if the system energy is conserved, the environment energy is not, since $[H_B, H_I] \neq 0$. The reduced state of the environment $\rho_E(t) = \text{Tr}_S[\rho_{SE}(t)]$ is a mixture of displaced thermal states

$$\rho_E(t) = \sum_j \rho_{S,jj}(0) \prod_k D(\alpha_k^j(t)) \rho_E(0) D(-\alpha_k^j(t)). \quad (10)$$

We can evaluate the energy of the bath:

$$\begin{aligned} \langle H_E(t) \rangle &= \text{Tr}_B[H_B \rho_E(t)] \\ &= \sum_j \rho_{S,jj}(0) \sum_k \omega_k \text{Tr}_k [b_k^\dagger b_k D(\alpha_k^j(t)) v_k D(-\alpha_k^j(t))] \\ &= \sum_j \rho_{S,jj}(0) \sum_k \omega_k \left(\frac{1}{e^{\omega_k/T} - 1} + |\alpha_k^j(t)|^2 \right). \end{aligned} \quad (11)$$

The absorbed heat is thus

$$Q(t) = \langle H_E(t) \rangle - \langle H_E(0) \rangle = \sum_j \rho_{S,jj}(0) \sum_k \omega_k |\alpha_k^j(t)|^2, \quad (12)$$

where we see that the thermal contribution remains the same, and the absorbed energy only depends on the displacement due to the interaction with the qudit. Taking the continuous limit and using the definition (3) we obtain (see also Ref. [36])

$$Q(t) = 2 \left(\sum_j \rho_{S,jj}(0) g_j^2 \right) \underbrace{\int_0^\infty d\omega J(\omega) \frac{1 - \cos \omega t}{\omega}}_{\equiv \mathbb{Q}(t)}. \quad (13)$$

In Eqs. (9) and (13) we have highlighted the nontrivial time-dependent quantities $\Delta_T(t)$ and $\mathbb{Q}(t)$ that also encode all the dependence on the environment features, i.e., spectral density and temperature. The system operators $\rho_S(0)$ and A_S only affect the absorbed heat as a multiplicative factor; moreover, when $g_j^2 = g_k^2 \forall j, k$ the heat $Q(t)$ is independent of $\rho_S(0)$.

Equation (13) shows that the average heat absorbed by the environment is always positive, a generic feature of pure-dephasing models [36]; in this particular case it is also independent of the temperature. While this feature may seem puzzling, one should remember that there is no energy exchange between system and environment, and heat dissipation is due to switching the interaction on and off. Indeed, $Q(t)$ is equal to the work that must be performed to couple the system and the environment at time 0 and later decouple them at time t [48,49]. Thus, for probing schemes based on dephasing, the figure of merit we use to quantify invasiveness corresponds also to the work cost of the thermometry protocol (neglecting the cost of state preparation [51,52] and measurement [53,54]).

More generally it is possible to go beyond average quantities, and heat in quantum systems may be defined as a random variable via the two-point measurement scheme [55]. For the sake of simplicity, we will refer to the average $Q(t)$ as heat and to the variance $\delta^2 Q(t)$ as heat fluctuations, and we will consider only these two quantities. We relegate the details about this definition of heat, as well as an explicit calculation of the heat fluctuations for our model, to Appendix A. We report the result in the main text only for a two-level probe system in Eq. (14), but the generic expression is reported in Eq. (A9). Differently from the average heat, the fluctuations depend on the temperature of the environment.

C. Two-level probe with Ohmic-like spectral density

For the sake of concreteness, from now on we focus on a two-level probe, coupled through the operator $A_S = \lambda \sigma_z$, where λ is an adimensional interaction-strength parameter, i.e., $g_0 = -g_1 = \lambda$ in Eq. (9). This model has been used, for example, to describe an atomic impurity in a Bose-Einstein condensate [46,56,57]. The dephasing function reads $\Delta_{01}(t) = \Delta_{10}(t) = 4\lambda^2 \Delta_T(t)$, the absorbed heat $Q(t) = 2\lambda^2 \mathbb{Q}(t)$, and the heat fluctuations

$$\delta^2 Q(t) = 2\lambda^2 \int_0^\infty d\omega J(\omega) (1 - \cos \omega t) \coth\left(\frac{\omega}{2T}\right). \quad (14)$$

An analogous expression is reported also in Ref. [36]. The heat variance is proportional to the dephasing factor $\Delta_T(t)$ for a different spectral density, obtained by multiplying the original one by ω^2 , i.e., with an Ohmicity parameter s increased by 2 for the class we will now go on to consider. This also ensures that the asymptotic value of $\delta^2 Q(t)$ for $t \rightarrow \infty$ does not diverge, by leveraging on results on the finiteness of the dephasing function [58,59].

We further choose a spectral density of the form $J(\omega) = \omega(\omega/\omega_c)^{s-1} C(\omega, \omega_c)$, where s is the so-called Ohmicity parameter and distinguishes three regimes: Ohmic for $s = 1$,

sub-Ohmic for $0 < s < 1$, and super-Ohmic for $s > 1$. In the main text we present results for an exponential cutoff

$C(\omega, \omega_c) = e^{-\omega/\omega_c}$, which grants a closed-form expression for the dephasing function [12]²:

$$\begin{aligned} \Delta_0(t) &= \Gamma(s-1) \{1 - (\tilde{t}^2 + 1)^{\frac{1}{2} - \frac{s}{2}} \cos[(s-1) \arctan(\tilde{t})]\} \\ \Delta_T(t) &= \Delta_0(t) + \frac{(s-1)s\tilde{T}^{s-1}\Gamma(s-1)^2}{\Gamma(s+1)} [2\zeta(s-1, \tilde{T}+1) - \zeta(s-1, i\tilde{T} + \tilde{T}+1) - \zeta(s-1, -i\tilde{T} + \tilde{T}+1)], \end{aligned} \quad (15)$$

where $\zeta(s, a) = \sum_{n=0}^{\infty} \frac{1}{(n+a)^s}$ is the generalized (Hurwitz) zeta function, and we have introduced the adimensional $\tilde{t} = t\omega_c$ and $\tilde{T} = T/\omega_c$ for compactness. The absorbed heat (13) can also be obtained

$$\mathbb{Q}^{\text{exp}}(t) = \omega_c \Gamma(s) \left(1 - \frac{\cos[s \arctan(t\omega_c)]}{(t^2\omega_c^2 + 1)^{\frac{s}{2}}} \right), \quad (16)$$

where $\Gamma(s) = \int_0^{\infty} t^{s-1} e^{-t} dt$ is the Gamma function.

In Appendix B we show additional results for a Gaussian cutoff and a hard cutoff: the exchanged heat is obtained analytically, see Appendix B 1, while the dephasing function (9) by numerical integration. While some phenomenology is different, the main qualitative features remain valid for different cutoffs.

D. Thermometry as parameter estimation

Temperature is a parameter to be estimated by measuring the probe. The accuracy of the estimation is influenced by the measurement, formally a positive operator-valued measure (POVM), and by the estimator \tilde{T} processing the outcomes into a temperature estimate. Since temperature is an energy-scale parameter, it is common [3, 6, 60, 61] and arguably more appropriate [62] to consider the relative error $\Delta^2 \tilde{T}/T^2$ as an error quantifier or equivalently, its inverse, the signal-to-noise ratio (SNR), as an accuracy quantifier.

For unbiased estimators, the quantum Cramér-Rao bound (QCRB) [63, 64] gives

$$\frac{T^2}{\Delta^2 \tilde{T}} \leq MT^2 \mathcal{F}[\rho_T(t)] \equiv M \mathcal{R}_T(t), \quad (17)$$

where $\mathcal{F}[\rho_T]$ is the quantum Fisher information (QFI) of the state ρ_T for the parameter T , expressed as $\mathcal{F}[\rho_T] = \text{Tr}[\partial_T \rho_T L_T]$ with the Hermitian symmetric logarithmic derivative operator L_T defined by $2\partial_T \rho_T = L_T \rho_T + \rho_T L_T$, while M is the number of identical shots of the experiment. The bound can be saturated asymptotically for large M by optimal measurements and estimators. We have also introduced the quantum signal-to-noise ratio (QSNR) [65] $\mathcal{R}_T \equiv T^2 \mathcal{F}[\rho_T]$, which will be our main figure of merit. Since the QCRB is attainable, the inverse of the QSNR \mathcal{R}_T^{-1} represents the optimal relative error in the regime of a large number of

shots; we will often refer to this quantity as the relative error (omitting “optimal” for brevity).

For a two-level probe in the initial state $\cos(\theta/2)|0\rangle + \sin(\theta/2)|1\rangle$ we have

$$\mathcal{F}[\rho_T(t)] = \frac{[\sin \theta 4\lambda^2 \partial_T \Delta_T(t)]^2}{\exp[8\lambda^2 \Delta_T(t)] - 1}, \quad (18)$$

and the QCRB is attained by a projective measurement on σ_x eigenstates [12]. A balanced superposition $\theta = \pi/2$ is the optimal probe state and will always be considered. Finding the optimal state is not as straightforward for higher-dimensional probe systems; we will briefly discuss this aspect in Sec. III B 2.

III. THERMOMETRIC PERFORMANCE VERSUS ABSORBED HEAT

A. Dynamics of thermometric accuracy and absorbed heat

In Fig. 1 we plot the QSNR and the absorbed heat as functions of the probing time. The parameter values for the plots are chosen to highlight a few different features that these figures of merit can display. First of all, the probe-sample interaction in this model is responsible both for imprinting the information about the temperature on the probe and for increasing the mean energy of the sample. Consequently, during the initial part of the dynamics there is always a tradeoff between invasiveness and relative error: to increase the accuracy we must allow the sample to absorb some heat. Even if the heat is always positive, it may display a nonmonotonic behavior in time, as highlighted, e.g., by the curve in panel (b1) for $s = 3$. However, $Q(t)$ settles to a finite asymptotic value $\lim_{t \rightarrow \infty} Q(t) \propto \lambda^2 \omega_c$. On the contrary, the QSNR can have a maximum in time and then decay to zero, as shown in panel (a1) for $s = 1$, when the asymptotic probe state has no coherence. In this case the parametric plot shows that after the initial trade-off region the QSNR does not increase even if we let the sample absorb more heat.

Otherwise, the QSNR can tend to a finite value, as shown in panel (b1) for $s = 3$ if the asymptotic probe state is not completely dephased, a phenomenon known as coherence trapping [59, 66]. In such situations the parametric plot in panel (b3) shows that after the initial tradeoff there may be regions in which both the absorbed heat and the error decrease simultaneously. This is due to the different timescales over which the two quantities vary appreciably, as highlighted by the panels (a1) and (b1) on the left of Fig. 1. Importantly, the key features of this analysis do not appreciably depend on the cut-off choice, as we show in Appendix B.

²This expression is slightly different from Eq. (17) in Ref. [12] due to some typos therein. Note also that the spectral density $J(\omega)$ is defined in that paper with an additional factor 4, and the results shown there are obtained by fixing $\lambda = 1/2$ in this work.

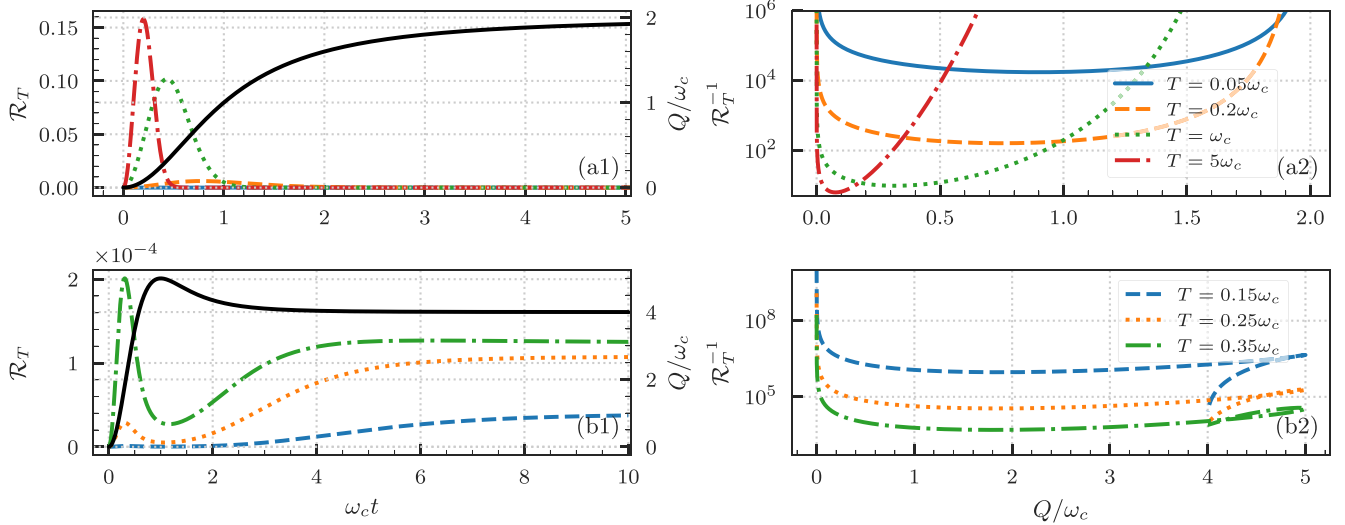


FIG. 1. Top [panels (a1) and (a2)]: Ohmic spectral density $s = 1$; bottom [panels (b1) and (b2)]: super-Ohmic spectral density $s = 3$; both for coupling $\lambda = 1$. Panels (a1) and (b1): absorbed heat (solid black line, units on the right) and quantum SNR (colored lines for various temperatures, units on the left) as a function of time. Panels (a2) and (b2): parametric plot of relative error for temperature estimation vs absorbed heat. Each line represents a different temperature, as shown in the legend.

Long-time asymptotic results

We have already shown that depending on the Ohmicity parameter, i.e., on the low-frequency behavior of the spectral density, it is possible to retain some coherence in the probe state even at asymptotically long times, preserving the ability to infer the temperature of the sample by measuring the asymptotic probe state. This happens for values $s > 2(1)$ at finite (zero) temperature [58], and here we focus on the case $T > 0$ and $s > 2$. For the exponential cutoff we were also able to obtain an expression for the asymptotic dephasing function $\Delta_T(\infty) \equiv \lim_{t \rightarrow \infty} \Delta_T(t)$ for $T > 0$ and $s > 2$ (while the integral diverges for $s \leq 2$):

$$\Delta_T(\infty) = 4\Gamma(s-1)[2\tilde{T}^{s-1}\zeta(s-1, \tilde{T}+1) + 1]. \quad (19)$$

While we were not able to derive this expression rigorously from (15) for all parameter values, we have obtained it analytically for integer values $s \geq 3$ and extrapolated it to other values of s , checking it matches numerical results. On other hand, the asymptotic value of the heat $Q(\infty) \equiv \lim_{t \rightarrow \infty} Q(t)$ is easily obtained and it is always finite:

$$Q(\infty) = 2\lambda^2\omega_c\Gamma(s); \quad (20)$$

it is not monotonic in s and reaches a minimum at $s_0 \approx 1.4616$.

In Fig. 2 we show the asymptotic thermometric accuracy $\mathcal{R}_T(\infty)$, obtained by using (19) to evaluate the QSNR, and the asymptotic absorbed heat $Q(\infty)$ in (20). We are restricted to the case $s > 2$, otherwise the asymptotic QSNR would be zero for $T > 0$. In this parameter region $Q(\infty)$ is monotonically increasing in s . On the contrary, we see that the QSNR reaches a maximum at particular values of s , which depend on the temperature. This means that increasing the Ohmicity from $s = 2$ towards larger values to increase the QSNR also increases the invasiveness until the optimal s is reached, but afterwards no gain in thermometric accuracy is obtained by allowing

a large amount of asymptotically absorbed heat. While, as usual, the absorbed heat does not depend on the temperature, the bottom panel of Fig. 2 shows the QSNR optimized over the Ohmicity parameter $\mathcal{R}_T^{\text{opt}}(\infty) \equiv \max_{s>2} \mathcal{R}_T(\infty)$. This optimized figure of merit has a dependence on the temperature; it goes to zero for large and small temperatures and has a maximum at some finite temperature. Overall the values of $\mathcal{R}_T^{\text{opt}}(\infty)$ are comparable to the values obtained at finite times for $s > 2$, see, e.g., panel (b1) of Fig. 1, even if the values obtained for $s < 2$ at finite time are generally much higher, see, e.g., panel (a1) of Fig. 1.

We remark that this method of operating a pure-dephasing thermometer, i.e., turning on the probe-sample interaction and waiting a long time so that a steady state is reached, resembles

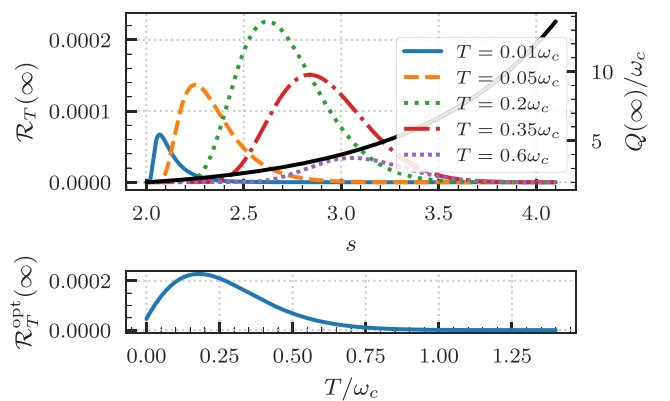


FIG. 2. Top panel: asymptotic absorbed heat (solid black line, units on the right) and asymptotic quantum SNR (colored lines for various temperatures, units on the left) as a function of the Ohmicity parameter s . Bottom panel: asymptotic quantum SNR optimized over Ohmicity s as a function of the temperature. In both panels the coupling strength is $\lambda = 1$.

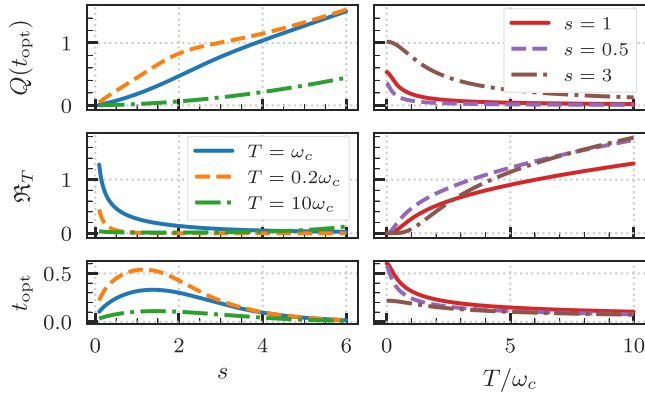


FIG. 3. Absorbed heat per shot (top panels), optimal QSNR rate (middle panels), and optimal probing time (bottom panels) as a function of s for $T/\omega_c = 0.2, 1, 10$ (left panels) and as a function of T for $s = 1/2, 1, 3$ (right panels). In both cases $\lambda = 1$.

the approach of equilibrium thermometry, in which the probe is measured after reaching a steady state and thermalizing with the sample. However, we stress that we are considering an interaction that does not involve direct energy exchanges between the probe and the sample and thus no thermalization of the probe ever occurs.

B. Time-optimal schemes

In absence of coherence trapping the QSNR reaches a maximum at a finite time and then decreases to zero, so it is beneficial to restrict to relatively short interactions, both to minimize the relative error and the invasiveness. Otherwise, it may instead be beneficial to let the probe and sample interact for long times. However, this conclusion does not take into account the fact that time is a valuable resource in quantum probing. Thus, we now focus on time-optimal schemes, with the aim to quantify the invasiveness in this practically relevant scenario.

The probing time t of each experiment can be chosen optimally, corresponding then to a total number of experiments $M = \tau/t$ (assuming the time for state preparation and measurement is negligible); this approach is standard in frequency estimation [67–69]. Time-optimal quantum thermometry has been studied, but considering a Markovian semigroup evolution [3,70], is generally unfit to capture the short-time dynamics of the probe [8].

According to the QCRB, the best accuracy obtainable in a total time τ is

$$\frac{T^2}{\Delta^2 \tilde{T}} \leq \tau \max_t \frac{\mathcal{R}_T}{t} \equiv \tau \mathfrak{R}_T, \quad (21)$$

attainable in the limit $\tau \gg t$ when the experiment is repeated many times. The optimal QSNR rate \mathfrak{R}_T is the relevant figure of merit for time-optimal schemes; the time $t_{\text{opt}} = \text{argmax}_t \frac{\mathcal{F}[\rho_T(t)]}{t}$ is the optimal duration of each shot of the experiment and plays an important role.

We study time-optimal schemes by performing the t optimization in Eq. (21) numerically. In Fig. 3 we show the optimal QSNR rate \mathfrak{R}_T and the heat $Q(t_{\text{opt}})$ absorbed during

each shot of the experiment, both as a function of s for three values of T in the panels on the left, and as a function of T for the three Ohmicity regimes in the panels on the right. We also plot the corresponding optimal probing time t_{opt} . Notice that $Q(t_{\text{opt}})$ depends on the temperature implicitly through t_{opt} .

From the results in Fig. 3 we see that for decreasing s the thermometric accuracy increases and the absorbed heat decreases. A similar behavior appears for increasing temperature. Thus, while time-optimal thermometry is not tailored to minimize the invasiveness, it is effective to keep it under control, meaning that it is possible to increase the accuracy, e.g., by decreasing s , without increasing the invasiveness.

As a side remark, we note that small values of s are in general beneficial in the low-temperature regime to increase the thermometric accuracy and not just for time-optimal protocols, as already hinted by the previous results. Indeed, at the lowest order in T we have $\mathcal{R}_T \propto T^{2(s+1)}$ (the full expression is involved and not particularly instructive but can be obtained analytically). This means that the QFI always goes to zero as $T \rightarrow 0$ for $s > 0$ and thus the absolute error diverges. We note that for other probe-sample interactions one can actually find a vanishing absolute error in the limit $T \rightarrow 0$, while the relative error always diverges [71].

1. Role of the coupling strength

The very idea to use quantum probes might *a priori* suggest that a small, albeit indeed non-negligible, coupling strength λ should be preferable to reduce the impact of the probe on the sample. However, by taking into account the invasiveness of the probe, we show that this is not necessarily the case. In physical systems the coupling strength can often be tuned to some extent; for example, when the model describes an impurity in a Bose-Einstein condensate, λ is related to the scattering length [46].

On the one hand, a stronger coupling increases the amount of heat absorbed by the environment, keeping everything else fixed, since it appears as an overall multiplicative factor in Eq. (13). On the other hand, it also makes the probe lose coherence faster, leading to a shorter optimal probing time during which less heat is absorbed. As shown in Fig. 4, the overall behavior is favorable for large λ . While Fig. 4 shows that the quantities are not monotonic in λ , as evidenced by the low-temperature curves in the region $0 < \lambda < 1$, we see that as λ increases the absorbed heat and also the fluctuations $\delta^2 Q(t_{\text{opt}})$ saturate to a constant, while the optimal QSNR rate increases linearly with λ . This happens because the optimal time decreases sufficiently fast as a function of λ ; this also has the effect that $Q(t_{\text{opt}})$ tends to a small fraction of its maximum possible $\max_t Q(t)$ for $\lambda = 1$. While Fig. 4 shows results for $s = 1$, in Appendix B we show that the large- λ behavior generally holds also for sub-Ohmic and super-Ohmic spectral densities.

Assuming that the optimal time is short, which is true for λ large enough, we can expand around $t = 0$ both the absorbed heat $Q(t)$ and the QFI. Quite generally, the first two lowest-order terms are quadratic and quartic, a behavior connected to the so-called Zeno regime of open quantum systems [68,72,73]. It is paramount to keep also the fourth-order contribution to have a nonmonotonic time dependence

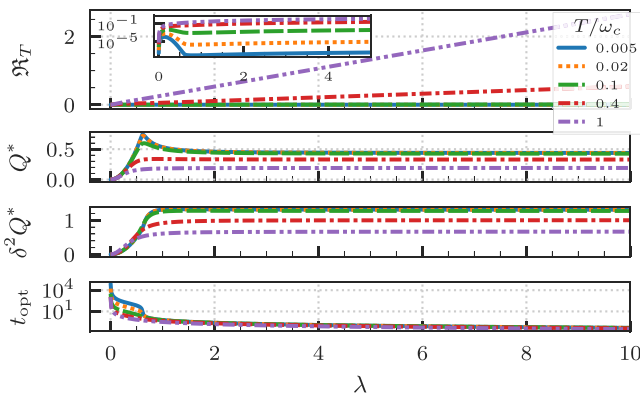


FIG. 4. Time-optimal QSNR rate (top panel, the inset is in logarithmic scale), average absorbed heat per shot $Q^* \equiv Q(t_{\text{opt}})$ (second panel from above), heat fluctuations at the optimal time $\delta^2 Q^* \equiv \delta^2 Q(t_{\text{opt}})$ (third panel from above), and optimal time (bottom panel) as a function of λ for $s = 1$ and several temperature values, shown in the legend.

and investigate the behavior of the optimal probing time.³ From this optimization we obtain that $t_{\text{opt}} \propto 1/\lambda$ for large λ and thus $Q(t)$ tends to a constant as λ increases, while \mathfrak{R}_T grows linearly; see Appendix D for details. While the role of coupling strength in quantum thermometry was studied in different models and with different outcomes [15,46,74], time-optimal schemes were not considered.

2. Higher-spin probes

Going beyond two-level probes, we study time-optimal dephasing thermometry with a spin- j probe, coupled to the sample via the operator $A_S = 2\lambda J_z$. In the simplest case, by initializing the probe in a spin cat state $(|j, j\rangle + |j, -j\rangle)/\sqrt{2}$ the whole dynamics is fully equivalent to a spin- $\frac{1}{2}$, i.e., a two-level, probe under the scaling $\lambda \mapsto 2j\lambda$, since the probe system remains in a two-dimensional subspace. For this initial condition, increasing the spin j is equivalent to increasing the coupling strength λ for a two-level probe. However, while for a two-level probe the optimal initial state is trivially a balanced superposition, for $j > 1/2$ the choice of a spin cat probe state is not necessarily optimal.

To study the truly optimal thermometric performance in this scenario, we numerically optimize the QFI rate over initial probe states by considering the quantity

$$\mathfrak{R}_T^{\text{max}} = \max_t \left\{ \frac{1}{t} \max_{|\psi_{SA}\rangle} \mathcal{F}[\mathcal{E}_{T,t} \otimes \mathcal{I}_A(|\psi_{SA}\rangle\langle\psi_{SA}|)] \right\}, \quad (22)$$

where $\mathcal{E}_{T,t}$ is the completely positive trace-preserving map, i.e., a dephasing quantum channel, that describes the reduced dynamics of the system S interacting with the sample. Here \mathcal{I}_A is the identity channel on an auxiliary system A , which is treated as an ideal quantum memory that does not undergo any evolution, and the initial pure state of S and A can be entangled. $\mathfrak{R}_T^{\text{max}}$ is the ultimate metrological bound

for a quantum channel, and it can be evaluated numerically via semidefinite programming [75,76]. More details on this procedure, including the explicit form of the channel $\mathcal{E}_{T,t}$, its Kraus representation, and the derivatives of the Kraus operators, are relegated to Appendix C.

We show that, in some regimes, spin cat states are optimal and match the ultimate metrological bounds for quantum channels [75,76]. In particular, spin cat probes become optimal when λ is large, and thus we suspect they may be optimal also when j is large (for a fixed λ), beyond what we can reach with our numerics.

IV. DISCUSSION AND OUTLOOK

We have analyzed a dephasing thermometry protocol, taking into consideration both the information encoded in the probe and the transformation of the sample due to the interaction with the probe, i.e., the invasiveness. In optical quantum metrology, invasiveness is related to the amount of light absorbed by optical samples [77,78]; similarly, we have quantified invasiveness in quantum thermometry with the amount of heat absorbed by the sample.

We have shown that to increase the thermometric accuracy as quantified by the QSNR, it is necessary to let the sample absorb a certain amount of heat. However, since the two quantities have in general a different behavior, both as functions of time and of the model parameters, there is no simple relation between them. This means that while the thermometry scheme is necessarily invasive to some extent, the parameter regions where the thermometric accuracy is higher do not necessarily correspond to the most invasive situations. This is particularly evident for time-optimal schemes, for which we have shown that minimizing the relative error generally also limits the absorbed heat. This happens also in regimes that may be thought to be invasive, such as very strong coupling. As a matter of fact, we have shown that this regime is useful because the temperature information is encoded quickly onto the probe state, and this compensates the fact that the absorbed heat at a fixed time increases with coupling strength.

Beyond pure dephasing, it will be interesting to study invasiveness when the probe's energy can change, e.g., using quantum thermal machines as thermometers [79,80]. Interestingly, even for interactions that allow energy exchanges, an equivalence between average work for coupling and decoupling and dissipated heat has been observed for short times [81]. Similarly, it is believed that dephasing effects arise on much shorter timescales than dissipation for open quantum systems [82]. These observations motivate further research on this topic, such as understanding the possibility of optimizing over time-dependent couplings.

Quantifying invasiveness with the energy increase of the environment will be particularly relevant for thermometry of many-body samples in pure states: temperature is directly related to the sample energy, and dephasing probes have been proposed as thermometers [83]. Further, invasiveness could also be characterized by considering the postmeasurement state [84] and extended to thermometry with sequential measurements [85,86].

As a final comment, we stress that energetic efficiency will become a relevant issue for quantum technologies [87]. The

³This is similar to the ‘‘Zeno time’’ defined in Ref. [89].

problem of quantifying and optimizing the energetic costs of quantum metrology protocols has received some attention [51,52], but this endeavor is in early stages. Our work is also a first step in this direction for dephasing quantum thermometry, since the heat absorbed by the environment coincides with the external work for coupling and decoupling the probe.

ACKNOWLEDGMENTS

We thank C. Benedetti, A. Candeloro, and A. Saltini for fruitful discussions. The authors acknowledge financial support from MUR under the ‘‘PON Ricerca e Innovazione 2014-2020’’ project EEQU.

APPENDIX A: HEAT FLUCTUATIONS IN THE TWO-POINT MEASUREMENT SCHEME

Following the two-point energy measurement scheme [36,55], we assume that the initial state is diagonal in the energy eigenbasis, and we define heat as the random variable with distribution

$$p(Q) = \sum_{m,n} p_n p_{m|n} \delta(Q + E_n - E_m), \quad (\text{A1})$$

where p_n is the initial probability of measuring the value E_n for the environment energy and $p_{m|n}$ is the conditional probability of measuring the environment energy E_m at the final time t , given the initial energy E_n , i.e.,

$$\rho_E(0) = \sum_n p_n \Pi_n \quad H_E = \sum_n E_n \Pi_n \quad p_{m|n} = \text{Tr}[\Pi_m U_{SE}(t) \rho_S(0) \otimes \Pi_n U_{SE}(t)^\dagger], \quad (\text{A2})$$

where Π_n are projectors onto energy E_n eigenspaces, and moreover, $p_n = e^{-\beta E_n} / Z_T$, since the initial state is assumed to be thermal.

The first and second moments of this random variable correspond to those of the observable $H_E(t) - H_E(0)$ (the time argument means that the operators are evolved in Heisenberg picture). The average heat $Q(t)$ corresponds to $\text{Tr}[\rho_E(0)(H_E(t) - H_E(0))]$ by definition, while one can check explicitly that the second moment is

$$\sum_m Q^2 p(Q) = \text{Tr}[H_E^2 \rho_{SE}(t)] + \text{Tr}[H_E^2 \rho_{SE}(0)] - 2\langle H_E(t) H_E(0) \rangle = \text{Tr}[\rho_E(0)(H_E(t) - H_E(0))^2], \quad (\text{A3})$$

and thus the variance is

$$(\delta Q(t))^2 = \Delta^2 H_E(t) + \Delta^2 H_E(0) - 2(\langle H_E(t) H_E(0) \rangle - \langle H_E(t) \rangle \langle H_E(0) \rangle). \quad (\text{A4})$$

The evaluation of these terms is straightforward but a bit lengthy. For the first term we obtain

$$\begin{aligned} \langle H_E^2(t) \rangle &= \text{Tr}_E[H_E^2 \rho_E(t)] = \sum_j \rho_{S,jj}(0) \left\{ \sum_k \omega_k^2 \left[\frac{1}{(e^{\omega_k/T} - 1)^2} + \frac{1}{e^{\omega_k/T} - 1} + |\alpha_k^j(t)|^2 \coth\left(\frac{\omega_k}{2T}\right) \right] \right. \\ &\quad \left. + \sum_{k,k'} \omega_k \left(\frac{1}{e^{\omega_k/T} - 1} + |\alpha_k^j(t)|^2 \right) \omega_{k'} \left(\frac{1}{e^{\omega_{k'}/T} - 1} + |\alpha_{k'}^j(t)|^2 \right) \right\}, \end{aligned} \quad (\text{A5})$$

where we have used thermal expectation values obtained, e.g., from the characteristic function of a thermal displaced state $\chi(\xi) = \text{Tr}[D(\xi)D(\alpha)\nu D(-\alpha)] = \exp[-\frac{1}{2}|\xi|^2 \coth(\frac{\omega}{2T})] \exp[\xi\alpha - \alpha\xi^*]$ as $\langle a^{\dagger m} a^n \rangle = (-1)^n \frac{\partial^{n+m}}{\partial \xi^m \partial \xi^{*n}} \chi(\xi)$. The second term is simpler, since it only depends on the initial state

$$\langle H_E^2(0) \rangle = \text{Tr}_B[H_B^2 \rho_E(0)] = \sum_k \omega_k^2 \left[\frac{1}{(e^{\omega_k/T} - 1)^2} + \frac{1}{e^{\omega_k/T} - 1} \right] + \sum_{k,k'} \omega_k \left(\frac{1}{e^{\omega_k/T} - 1} \right) \omega_{k'} \left(\frac{1}{e^{\omega_{k'}/T} - 1} \right). \quad (\text{A6})$$

Finally, the third term is

$$\begin{aligned} \langle H_E(t) H_E(0) \rangle &= \text{Tr}[H_B U_I(t) H_B \rho_S(0) \otimes \rho_E(0) U_I^\dagger(t)] = \sum_j \rho_{S,jj}(0) \left\{ \sum_k \omega_k^2 \left(\frac{1}{(e^{\omega_k/T} - 1)^2} + \frac{1}{e^{\omega_k/T} - 1} \right) \right. \\ &\quad \left. + \sum_{k,k'} \omega_k \left(\frac{1}{e^{\omega_k/T} - 1} + |\alpha_k^j(t)|^2 \right) \omega_{k'} \left(\frac{1}{e^{\omega_{k'}/T} - 1} \right) \right\}. \end{aligned} \quad (\text{A7})$$

Putting everything together we obtain

$$\begin{aligned} \sum_m Q^2 p(Q) &= \sum_j \rho_{S,jj}(0) \left\{ \sum_k \omega_k^2 |\alpha_k^j(t)|^2 \coth\left(\frac{\omega_k}{2T}\right) + \sum_{k,k'} \omega_k \omega_{k'} \left[\left(\frac{1}{e^{\omega_k/T} - 1} + |\alpha_k^j(t)|^2 \right) \left(\frac{1}{e^{\omega_{k'}/T} - 1} + |\alpha_{k'}^j(t)|^2 \right) \right. \right. \\ &\quad \left. \left. + \left(\frac{1}{e^{\omega_k/T} - 1} \right) \left(\frac{1}{e^{\omega_{k'}/T} - 1} \right) - 2 \left(\frac{1}{e^{\omega_k/T} - 1} + |\alpha_k^j(t)|^2 \right) \left(\frac{1}{e^{\omega_{k'}/T} - 1} \right) \right] \right\} \end{aligned} \quad (\text{A8})$$

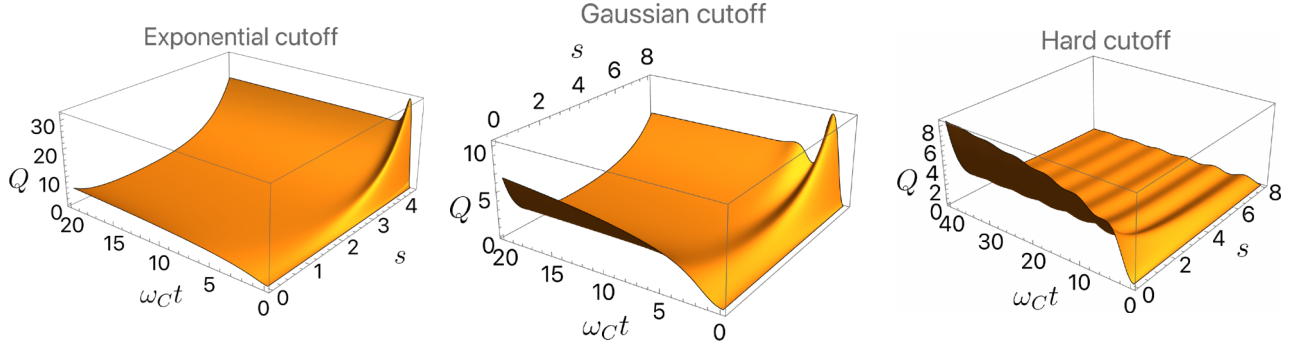


FIG. 5. Absorbed heat (in units of ω_c) for Ohmic-like spectral densities, as a function of evolution time and Ohmicity parameter s , for three choices of cut-off functions.

and

$$\begin{aligned}
 (\delta Q)^2 = & 2 \left(\sum_j \rho_{s,jj}(0) g_j^2 \right) \sum_k |f_k|^2 (1 - \cos \omega_k t) \coth \left(\frac{\omega_k}{2T} \right) + 4 \left[\sum_j \rho_{s,jj}(0) g_j^4 - \left(\sum_j \rho_{s,jj}(0) g_j^2 \right) \left(\sum_{j'} \rho_{s,j'j'}(0) g_{j'}^2 \right) \right] \\
 & \times \sum_{k,k'} |f_k|^2 |f_{k'}|^2 \frac{(1 - \cos \omega_k t)(1 - \cos \omega_{k'} t)}{\omega_k \omega_{k'}}. \quad (\text{A9})
 \end{aligned}$$

Taking the continuum limit for a spin-1/2 particle with σ_z coupling (i.e., $g_0 = -g_1 = \lambda$) we obtain Eq. (14), which matches with Eq. (47) in Ref. [36]. (The different numerical prefactor is due to the coupling operator being the spin operator $\sigma_z/2$ and to the interaction strength λ being included in $J(\omega)$.)

APPENDIX B: ADDITIONAL RESULTS FOR OTHER SPECTRAL DENSITIES

In this Appendix we present additional plots for different spectral densities than those considered in the main text. We explore Gaussian and hard cut-off functions and different Ohmicity parameters.

Overall, we observe that the key qualitative observations presented in the main text remain valid, while some finer details depend on these features of the spectral density. Such observation can be summed up as follows:

(a) A tradeoff between absorbed heat and relative error for short times

(b) For intermediate and long times the detailed relationship between the two quantities is less clear and depends on whether the spectral density under consideration allows for coherence trapping or not. Note that the presence of coherence trapping depends on s and is independent of the cut-off function, since it is related to the low-frequency behavior of $J(\omega)$ as $\omega \rightarrow 0$.

(c) For time-optimal schemes it is beneficial to have smaller values of s , since it decreases both the relative error and the disturbance.

(d) For time-optimal schemes it is beneficial to go to very large coupling values λ .

Before showing the results mentioned above, in Appendix B 1 we present a comparison between the absorbed heat with the three different cutoffs. These expressions can be obtained analytically and depend only on the time and Ohmicity parameter; this is instructive to see some of the different features induced by changing the cutoff function.

For the Gaussian and hard cutoffs we are able to evaluate the dephasing function analytically only for $T = 0$, since the integral is the same involved in the calculation of the absorbed heat, but the results for $T > 0$ employed in Appendixes B 2 and B 3 are obtained by numerical integration.

1. Absorbed heat comparison

For the considered model the absorbed heat depends non-trivially only on the evolution time and on the Ohmicity parameter, since λ^2 is only a multiplicative factor and there is no temperature dependence, as can be seen from (12) or Eq. (2) of the main text. This function of two parameters is shown in Fig. 5 for different cut-off functions. For the exponential cutoff the explicit expression is reported in Eq. (16), and we see that it tends to increase for large s at all times, while showing a peak for short times only in the super-Ohmic region. We also see that the asymptotic value is not monotonic in s , as reported in (20).

Also for the other cut-off functions the absorbed heat can be evaluated analytically. For a Gaussian cutoff $C(\omega, \omega_c) = e^{-\omega^2/\omega_c^2}$ we obtain

$$Q^{\text{Gauss}}(t) = \lambda^2 \omega_c \Gamma \left(\frac{s}{2} \right) \left\{ 1 - {}_1F_1 \left(\left[\frac{s}{2} \right]; \left[\frac{1}{2} \right]; -\frac{1}{4} t^2 \omega_c^2 \right) \right\}, \quad (\text{B1})$$

with the asymptotic value

$$\lim_{t \rightarrow \infty} Q^{\text{Gauss}}(t) = \lambda^2 \omega_c \Gamma \left(\frac{s}{2} \right). \quad (\text{B2})$$

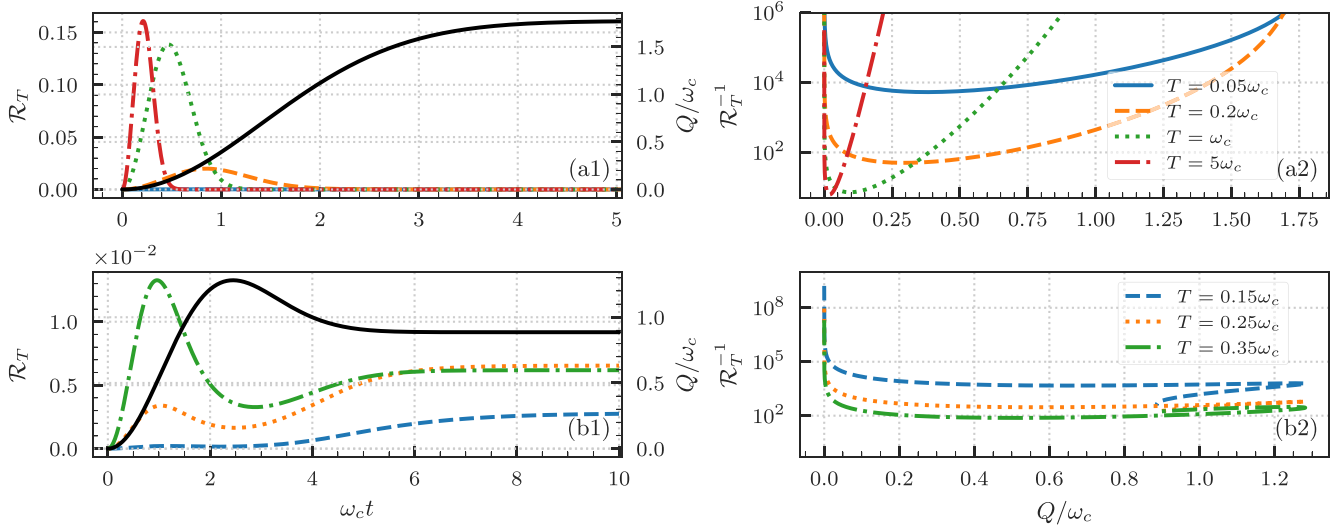


FIG. 6. Plots analogous to Fig. 1 in the main text, but for Ohmic-like spectral densities with a Gaussian cutoff. Top [panels (a)]: Ohmic spectral density $s = 1$; bottom [panels (b)]: super-Ohmic spectral density $s = 3$; both for coupling $\lambda = 1$. Panels (a1) and (b1): absorbed heat (solid black line, units on the right) and quantum SNR (colored lines for various temperatures, units on the left) as a function of time. Panels (a2) and (b2): parametric plot of relative error for temperature estimation vs absorbed heat. Each line represents a different temperature, as shown in the legend.

For the hard cutoff $C = \Theta(\omega_c - \omega)$, where $\Theta(s)$ is the Heaviside step function, we obtain

$$Q^{\text{hard}}(t) = \frac{2\lambda^2\omega_c [1 - {}_1F_2\left(\left[\frac{s}{2}\right]; \left[\frac{1}{2}, \frac{s}{2} + 1\right]; -\frac{1}{4}t^2\omega_c^2\right)]}{s}, \quad (\text{B3})$$

where ${}_pF_q(\vec{a}; \vec{b}; z) = \sum_{k=0}^{\infty} \frac{(a_1)_k \dots (a_p)_k}{(b_1)_k \dots (b_q)_k} \frac{z^k}{k!}$ is the generalized hypergeometric function and $(a)_k = \frac{\Gamma(a+k)}{\Gamma(a)}$ are Pochhammer symbols. The corresponding asymptotic value is

$$\lim_{t \rightarrow \infty} Q^{\text{hard}}(t) = \frac{2\lambda^2\omega_c}{s}. \quad (\text{B4})$$

The nontrivial dependence on the parameters s and t for these other two cut-off functions is shown in Fig. 5. There are some qualitative differences between the heat for different cut-off functions, the most important being that for a hard cutoff we see oscillations and the absorbed heat tends to zero for large s .

2. Thermometric performance versus heat as a function of time

In Figs. 6 and 7 we reproduce the plot in Fig. 1, but for a Gaussian and a hard cutoff, respectively. The main qualitative features are the same. There is an initial tradeoff between absorbed heat and QSNR at short times, since both quantities start from zero. The heat does not decrease back to zero asymptotically, while the QSNR does for $s = 1$, but not for $s = 3$ when trapped coherences are present in the probe. The main qualitative difference is that for a hard cutoff an oscillatory behavior for sufficiently long times can be observed, which is not present for Gaussian and exponential cutoffs. Despite such qualitatively different behavior of the heat, the main conclusions regarding the relationship between heat and thermometric accuracy stated in the main text remain valid.

3. Time-optimal thermometry

In Fig. 8 we reproduce the plots in Fig. 4, but for a sub-Ohmic spectral density $s = 1/2$ and for a super-Ohmic spectral density $s = 3$. We see that the large- λ behavior highlighted in the main text, i.e., $Q(t_{\text{opt}})$ saturating to a finite value and \mathfrak{R}_T growing linearly, remains valid. However, we see that the behaviors for smaller values of λ are rather different, with the super-Ohmic case showing more peculiar features.

In Fig. 9 we reproduce again the plot in Fig. 4, keeping the Ohmicity parameter $s = 1$, but for Gaussian and hard cutoffs.

APPENDIX C: NUMERICAL EVIDENCE FOR THE OPTIMALITY OF SPIN CAT STATES

Before considering all the details of the temperature estimation problem in the main text, we need to consider the underlying problem of estimating a constant dephasing factor.

1. Evaluation of the optimal QFI for dephasing estimation

We focus on the estimation of a *constant* dephasing factor Δ characterizing a dephasing channel \mathcal{E}_Δ that acts as follows on a finite-dimensional system,

$$\begin{aligned} \mathcal{E}_\Delta[\rho] &= \sum_{i,j} \rho_{ij} e^{-\Delta(i-j)^2} |i\rangle\langle j| \equiv \mathbf{E}_\Delta \circ \rho \\ \mathbf{E}_\Delta &= \sum_{i,j} e^{-\Delta(i-j)^2} |i\rangle\langle j|, \end{aligned} \quad (\text{C1})$$

where \circ denotes the elementwise (Hadamard) product between two matrices; this is an instance of a so-called quantum Hadamard channel [90].

This channel encodes the ‘‘operatorial’’ part of the thermometry problem considered in the main text. The fact that

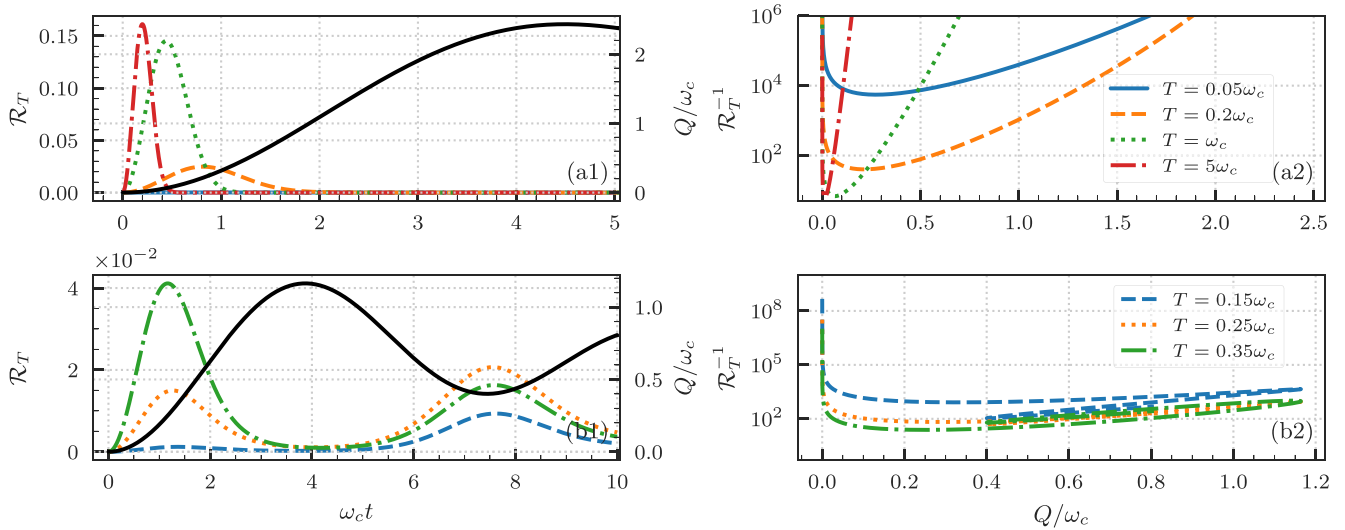


FIG. 7. Plots analogous to Fig. 1 in the main text, but for Ohmic-like spectral densities with a hard (step function) cutoff. Top [panels (a)]: Ohmic spectral density $s = 1$; bottom [panels (b)]: super-Ohmic spectral density $s = 3$; both for coupling $\lambda = 1$. Panels (a1) and (b1): absorbed heat (solid black line, units on the right) and quantum SNR (colored lines for various temperatures, units on the left) as a function of time. Panels (a2) and (b2): parametric plot of relative error for temperature estimation vs absorbed heat. Each line represents a different temperature, as shown in the legend.

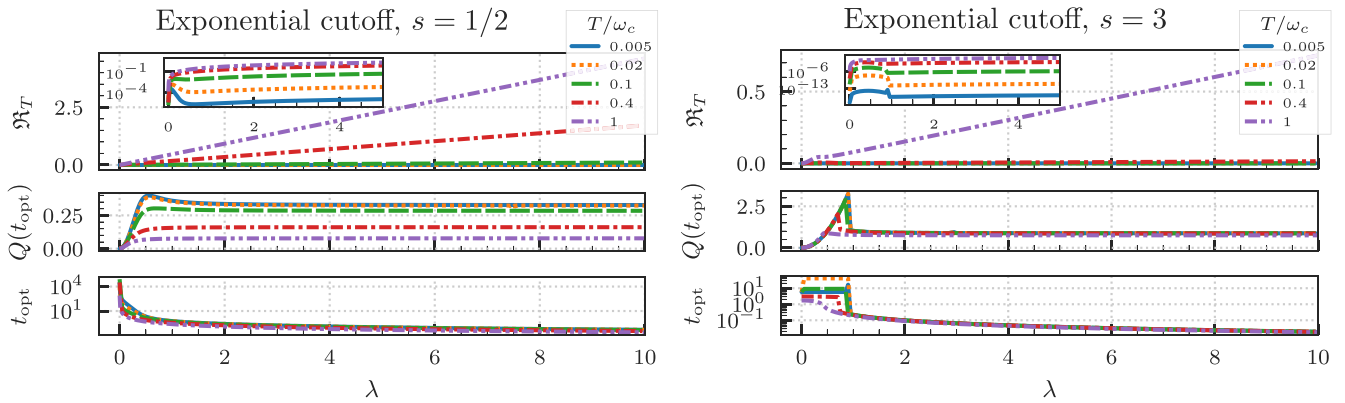


FIG. 8. Plots analogous to Fig. 3 in the main text, but for $s = 1/2$ (left) and $s = 3$. Time-optimal QSNR rate (top panels, the insets are in logarithmic scale), absorbed heat per shot (middle panels), and optimal time (bottom panels), all plotted as a function of λ for several temperature values, shown in the legend.

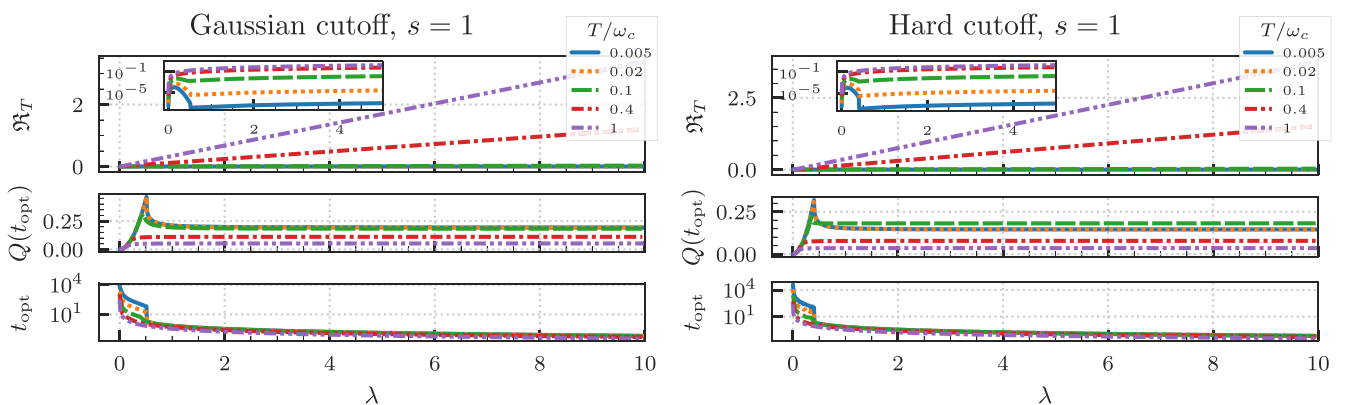


FIG. 9. Plots analogous to Fig. 4, but for a Gaussian (left) and hard (right) cutoff, both for $s = 1$ as in Fig. 4. Time-optimal QSNR rate (top panels, the inset is in logarithmic scale), absorbed heat per shot (middle panels), and optimal time (bottom panels) as a function of λ for several temperature values, shown in the legend.

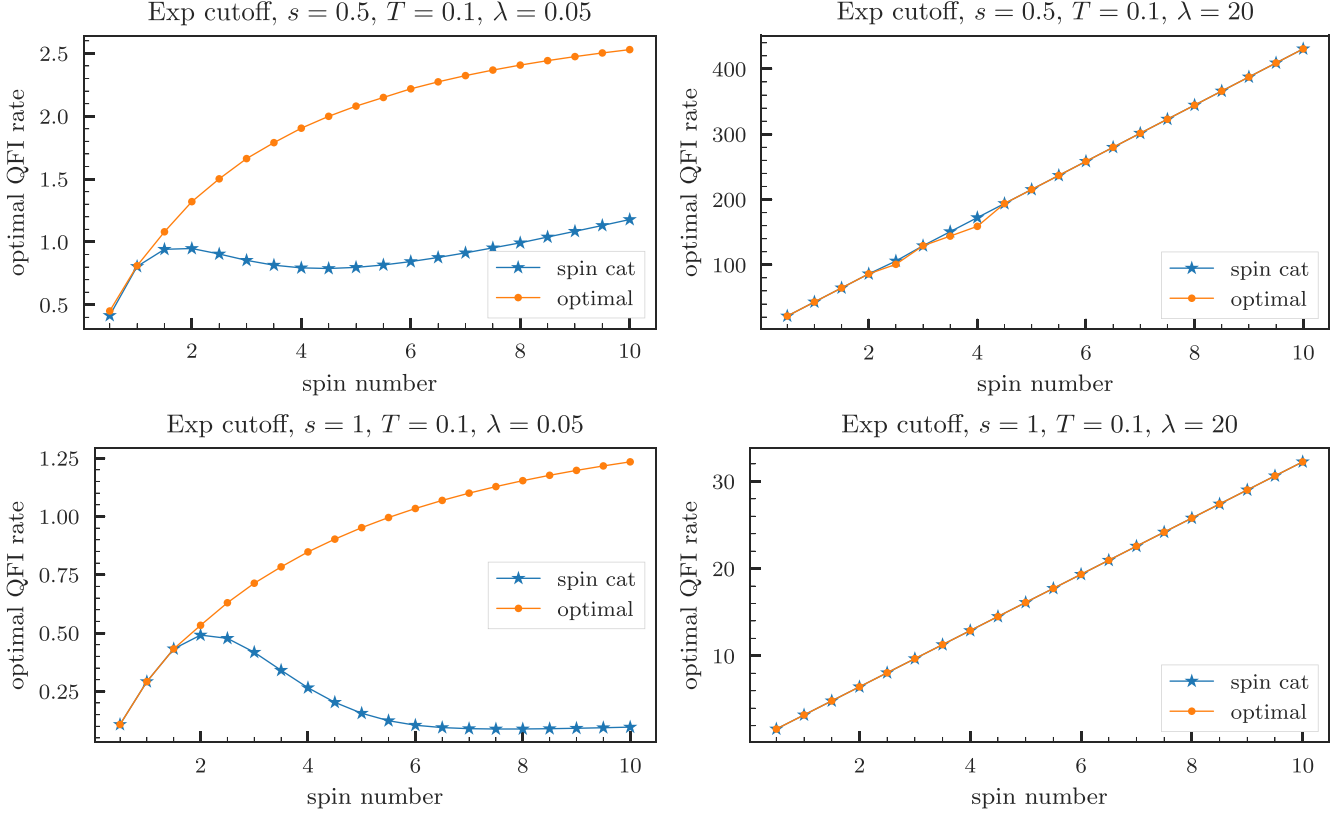


FIG. 10. Comparison between dephasing thermometry with optimal spin probes and with spin cat states.

Δ is actually a time-dependent function of the temperature appears in the QFI only as a multiplicative factor, which mainly plays a role in the optimization over the probing time. The dephasing matrix \mathbf{E}_Δ is essentially the Choi matrix of the channel, after removing redundant columns and rows of zeros.

To evaluate the optimal QFI we use the method introduced in Ref. [75] based on the optimization over equivalent Kraus representations $\{K_j\}_{j=1,\dots,r}$ of the dynamical map $\mathcal{E}_\Delta[\cdot] = \sum_{k=1}^r K_k \cdot K_k^\dagger$ that encodes the parameter. Explicitly, it can be evaluated as the minimization over a Hermitian matrix of size $r \times r$ of a quadratic function of h involving the Kraus operators and their derivatives:

$$\begin{aligned} \mathfrak{F}(\Delta) &= \max_{|\psi\rangle_{SA}} \mathcal{F}[\mathcal{E}_\Delta \otimes \mathcal{I}_A(|\psi_{SA}\rangle\langle\psi_{SA}|)] \\ &= 4 \min_{h=h^\dagger} \left\| \sum_k \left(\dot{K}_k - i \sum_j h_{kj} K_j \right)^\dagger \right. \\ &\quad \left. \times \left(\dot{K}_k - i \sum_{j'} h_{kj'} K_{j'} \right) \right\|. \end{aligned} \quad (\text{C2})$$

Here we see that the quantity evaluated by this method is not only an optimization over initial states of the system but also includes the possibility of using a noiseless ancillary system of arbitrary dimension and initial entangled states. If the noiseless ancillary system is not available, the quantity in Eq. (C2) is generally just an upper bound. Crucially, this minimization

can be evaluated numerically by solving a semidefinite program [76].

Given a spectral decomposition of the (real, positive semidefinite) dephasing matrix $\mathbf{E}_\Delta = \sum_{j=1}^d \kappa_j \mathbf{k}_j \mathbf{k}_j^T$, one can write a Kraus representation made of diagonal operators

$$K_j = \sqrt{\kappa_j} \text{diag}(\mathbf{k}_j). \quad (\text{C3})$$

Since the derivative of the dephasing matrix $\dot{\mathbf{E}} \equiv \partial_\Delta \mathbf{E}_\Delta$ is known,

$$\begin{aligned} \partial_\Delta \mathcal{E}_\Delta[\rho] &= \sum_{i \neq j} \rho_{ij} (i-j)^2 e^{-\Delta(i-j)^2} |i\rangle\langle j| \equiv \dot{\mathbf{E}}_\Delta \circ \rho \\ \dot{\mathbf{E}} &= - \sum_{i \neq j} (i-j)^2 e^{-\Delta(i-j)^2} |i\rangle\langle j|, \end{aligned} \quad (\text{C4})$$

to compute the derivatives of the Kraus operators we need to evaluate the derivatives of the eigenvalues $\{\kappa_j\}$ and eigenvectors $\{\mathbf{k}_j\}$ through first-order perturbation theory:

$$\begin{aligned} \dot{\kappa}_j &= \mathbf{k}_j^T \dot{\mathbf{E}} \mathbf{k}_j, \quad \dot{\mathbf{k}}_j = \sum_{i \neq j} \frac{\mathbf{k}_i^T \dot{\mathbf{E}} \mathbf{k}_i}{\kappa_i - \kappa_j}, \\ \dot{K}_j &= \frac{\dot{\kappa}_j}{2\sqrt{\kappa_j}} \text{diag}(\mathbf{k}_j) + \sqrt{\kappa_j} \text{diag}(\dot{\mathbf{k}}_j). \end{aligned} \quad (\text{C5})$$

Summing up, we can evaluate the optimal QFI numerically by first diagonalizing the dephasing matrix in Eq. (C1), from which the Kraus operators and their derivatives can be evaluated through Eqs. (C3) and (C5), and in turn these

two sets of operators are fed to a semidefinite program that solves the minimization in Eq. (C2). While we have used this method for quantum thermometry, it could be applied to other estimation problems. For example, in Ref. [23] the similar problem of estimating a parameter appearing in the dephasing function of a many-qubit state was studied by numerically sampling random probe states, showing that in some regimes Greenberger-Horne-Zeilinger (GHZ) states (completely analogous to spin cat states, but considering multiqubit systems instead of a single spin- j system) are optimal, similarly to what we show next.

2. Comparison between time-optimal schemes with spin cat and optimal probe states

By employing the optimal QFI presented in the previous section to perform the time optimization, we obtain the ultimate performance achievable with spin- j probe states. The probe-optimized quantity in (22) is thus evaluated numerically through (C2) as

$$\mathfrak{R}_T^{\max} = \max_t \frac{1}{t} [4\lambda^2 \partial_T \Delta_T(t)]^2 \mathfrak{F}(4\lambda^2 \Delta_T(t)), \quad (\text{C6})$$

where the maximization over t is carried out using a Nelder-Mead algorithm, while the function $\mathfrak{F}(4\lambda^2 \Delta_T(t))$ is evaluated with a semidefinite program for each t .

Some of the results of this comparison are shown in Fig. 10. We see that for both $s = 1$ and $s = 0.5$, the performance of spin cat states coincides with the optimal result for very strong coupling (e.g., $\lambda = 20$ in the two right panels of Fig. 10). However, in the weak-coupling regime (e.g., $\lambda = 0.05$ in the two left panels) the spin cat states start as optimal, then become suboptimal with the optimal QFI rate that decreases as the spin number j increases, but after this decline the optimal QFI rate starts increasing again with j . Unfortunately, evaluating the quantity in Eq. (C6) for larger values of j is too computationally demanding. However, we suspect that

$$\Delta_{s,T}^{(2)} = \frac{2(s-1)s\Gamma(s-1)[2(s-1)sT^{s+1}\Gamma(s-1)\zeta(s+1, T+1) + \Gamma(s+1)]}{\Gamma(s+1)}, \quad (\text{D5})$$

$$\Delta_{s,T}^{(4)} = -\frac{[s(s^3 + 2s^2 - s - 2)\Gamma(s-1)(2(s-1)sT^{s+3}\Gamma(s-1)\zeta(s+3, T+1) + \Gamma(s+1))]}{6\Gamma(s+1)}, \quad (\text{D6})$$

from which the QFI reads

$$\mathcal{F}[\rho_T(t)] = \frac{16\lambda^4 [\partial_T \Delta_{s,T}(t)]^2}{\exp[8\lambda^2 \Delta_{s,T}(t)] - 1} = f^{(2)}t^2 + f^{(4)}t^4 + O(t^6) \quad (\text{D7})$$

$$f^{(2)} = \frac{\lambda^2 (\partial_T \Delta_{s,T}^{(2)})^2}{2\Delta_{s,T}^{(2)}} \quad (\text{D8})$$

$$f^{(4)} = -\frac{\lambda^4 (\Delta_{s,T}^{(2)})^2 (\partial_T \Delta_{s,T}^{(2)})^2 + \lambda^2 [\Delta_{s,T}^{(4)} (\partial_T \Delta_{s,T}^{(2)})^2 - 2\Delta_{s,T}^{(2)} \partial_T \Delta_{s,T}^{(2)} \partial_T \Delta_{s,T}^{(4)}]}{2(\Delta_{s,T}^{(2)})^2}. \quad (\text{D9})$$

eventually, for j large enough, spin cat probes may become optimal again, since for this class of states increasing j is equivalent to increasing λ , and for large λ we have shown that they are optimal. Similar conclusions may be found for different values of s and T .

A previous indication of the optimality of spin cat probes for the estimation of environmental parameters appearing in the dephasing factor was given⁴ in Ref. [23]. In particular, it was shown that for fixed j there is a threshold value, and if the dephasing is weak enough it is optimal to use spin cat states. We note, however, that the figure of merit optimized in Ref. [23] was the QFI and not the QFI rate. Moreover, for a fixed dephasing Δ , i.e., the quantum channel (C1), the optimal state for asymptotically large j is not a spin cat state [91]. However, for a time-dependent problem the scenario is quite different, since the optimal time also scales with j and the problem differs from the estimation of a fixed dephasing factor Δ .

APPENDIX D: SHORT-TIME EXPANSIONS

We report here the short-time expansions of absorbed heat, dephasing function, and QFI for the spectral density with exponential cutoff. For conciseness, we implicitly express t and T in units of ω_c . The heat reads

$$Q(t) = \lambda^2 [q^{(2)}t^2 + q^{(4)}t^4 + O(t^6)], \quad (\text{D1})$$

$$q^{(2)} = s(s+1)\Gamma(s), \quad (\text{D2})$$

$$q^{(4)} = -\frac{1}{12}(s^4 + 6s^3 + 11s^2 + 6s)\Gamma(s), \quad (\text{D3})$$

and the dephasing function

$$\Delta_{s,T}(t) = \Delta_{s,T}^{(2)}t^2 + \Delta_{s,T}^{(4)}t^4 + O(t^6), \quad (\text{D4})$$

⁴More precisely, Greenberger-Horne-Zeilinger states of multiqubit systems were considered instead of cat states of a spin- j system, but the analysis is equivalent.

As long as the coefficient $f^{(4)}$ is negative (this depends on the particular parameter values, but we can always find λ large enough for which this holds), the optimal time is

$$t_{\text{opt}} = \operatorname{argmax}_t \frac{\mathcal{F}[\rho_T(t)]}{t} = \sqrt{-\frac{f^{(2)}}{3f^{(4)}}}, \quad (\text{D10})$$

which approaches zero as λ^{-1} for $\lambda \rightarrow \infty$.

-
- [1] A. De Pasquale and T. M. Stace, in *Thermodynamics in the Quantum Regime: Fundamental Aspects and New Directions*, edited by F. Binder, L. A. Correa, C. Gogolin, J. Anders, and G. Adesso, Fundamental Theories of Physics (Springer International Publishing, Cham, Switzerland, 2018), pp. 503–527.
- [2] M. Mehboudi, A. Sanpera, and L. A. Correa, *J. Phys. A: Math. Theor.* **52**, 303001 (2019).
- [3] L. A. Correa, M. Mehboudi, G. Adesso, and A. Sanpera, *Phys. Rev. Lett.* **114**, 220405 (2015).
- [4] M. G. A. Paris, *J. Phys. A: Math. Theor.* **49**, 03LT02 (2016).
- [5] S. Campbell, M. G. Genoni, and S. Deffner, *Quantum Sci. Technol.* **3**, 025002 (2018).
- [6] P. P. Potts, J. B. Brask, and N. Brunner, *Quantum* **3**, 161 (2019).
- [7] M. Mehboudi, M. R. Jørgensen, S. Seah, J. B. Brask, J. Kołodyński, and M. Perarnau-Llobet, *Phys. Rev. Lett.* **128**, 130502 (2022).
- [8] H.-P. Breuer and F. Petruccione, *The Theory of Open Quantum Systems* (Oxford University Press, Oxford, England, 2002).
- [9] M. Brunelli, S. Olivares, M. Paternostro, and M. G. A. Paris, *Phys. Rev. A* **86**, 012125 (2012).
- [10] A. H. Kiilerich, A. De Pasquale, and V. Giovannetti, *Phys. Rev. A* **98**, 042124 (2018).
- [11] V. Cavina, L. Mancino, A. De Pasquale, I. Gianani, M. Sbroscia, R. I. Booth, E. Roccia, R. Raimondi, V. Giovannetti, and M. Barbieri, *Phys. Rev. A* **98**, 050101(R) (2018).
- [12] S. Razavian, C. Benedetti, M. Bina, Y. Akbari-Kourbolagh, and M. G. A. Paris, *Eur. Phys. J. Plus* **134**, 284 (2019).
- [13] M. M. Khan, M. Mehboudi, H. Terças, M. Lewenstein, and M. A. Garcia-March, *Phys. Rev. Res.* **4**, 023191 (2022).
- [14] D.-J. Zhang and D. M. Tong, *npj Quantum Inf.* **8**, 81 (2022).
- [15] M. T. Mitchison, T. Fogarty, G. Guarnieri, S. Campbell, T. Busch, and J. Goold, *Phys. Rev. Lett.* **125**, 080402 (2020).
- [16] L. Oghittu and A. Negretti, *Phys. Rev. Res.* **4**, 023069 (2022).
- [17] G. Mihailescu, S. Campbell, and A. K. Mitchell, *Phys. Rev. A* **107**, 042614 (2023).
- [18] S. Campbell and B. Vacchini, *Europhys. Lett.* **133**, 60001 (2021).
- [19] S. Seah, S. Nimmrichter, D. Grimmer, J. P. Santos, V. Scarani, and G. T. Landi, *Phys. Rev. Lett.* **123**, 180602 (2019).
- [20] A. Shu, S. Seah, and V. Scarani, *Phys. Rev. A* **102**, 042417 (2020).
- [21] E. O'Connor, B. Vacchini, and S. Campbell, *Entropy* **23**, 1634 (2021).
- [22] C. Benedetti, F. Buscemi, P. Bordone, and M. G. A. Paris, *Phys. Rev. A* **89**, 032114 (2014).
- [23] M. A. C. Rossi and M. G. A. Paris, *Phys. Rev. A* **92**, 010302(R) (2015).
- [24] M. Bina, F. Grasselli, and M. G. A. Paris, *Phys. Rev. A* **97**, 012125 (2018).
- [25] D. Tamascelli, C. Benedetti, H.-P. Breuer, and M. G. A. Paris, *New J. Phys.* **22**, 083027 (2020).
- [26] C. L. Degen, F. Reinhard, and P. Cappellaro, *Rev. Mod. Phys.* **89**, 035002 (2017).
- [27] P. Szańkowski, G. Ramon, J. Krzywdka, D. Kwiatkowski, and Ł. Cywiński, *J. Phys.: Condens. Matter* **29**, 333001 (2017).
- [28] Y.-X. Wang and A. A. Clerk, *Nat. Commun.* **12**, 6528 (2021).
- [29] M. Hohmann, F. Kindermann, T. Lausch, D. Mayer, F. Schmidt, and A. Widera, *Phys. Rev. A* **93**, 043607 (2016).
- [30] Q. Bouton, J. Nettersheim, D. Adam, F. Schmidt, D. Mayer, T. Lausch, E. Tiemann, and A. Widera, *Phys. Rev. X* **10**, 011018 (2020).
- [31] D. Adam, Q. Bouton, J. Nettersheim, S. Burgardt, and A. Widera, *Phys. Rev. Lett.* **129**, 120404 (2022).
- [32] K. Ptaszyński and M. Esposito, *Phys. Rev. Lett.* **123**, 200603 (2019).
- [33] D. Gribben, A. Strathearn, J. Iles-Smith, D. Kilda, A. Nazir, B. W. Lovett, and P. Kirton, *Phys. Rev. Res.* **2**, 013265 (2020).
- [34] M. Brenes, J. J. Mendoza-Arenas, A. Purkayastha, M. T. Mitchison, S. R. Clark, and J. Goold, *Phys. Rev. X* **10**, 031040 (2020).
- [35] D. Tamascelli, *Entropy* **22**, 1320 (2020).
- [36] M. Popovic, M. T. Mitchison, A. Strathearn, B. W. Lovett, J. Goold, and P. R. Eastham, *PRX Quantum* **2**, 020338 (2021).
- [37] T. Chen and D. Poletti, *Phys. Rev. E* **104**, 054118 (2021).
- [38] K. Ptaszyński and M. Esposito, *Phys. Rev. E* **106**, 014122 (2022).
- [39] D. Gribben, A. Strathearn, G. E. Fux, P. Kirton, and B. W. Lovett, *Quantum* **6**, 847 (2022).
- [40] M. Wiedmann, J. T. Stockburger, and J. Ankerhold, *New J. Phys.* **22**, 033007 (2020).
- [41] G. T. Landi and M. Paternostro, *Rev. Mod. Phys.* **93**, 035008 (2021).
- [42] P. Talkner and P. Hänggi, *Rev. Mod. Phys.* **92**, 041002 (2020).
- [43] A. J. Leggett, S. Chakravarty, A. T. Dorsey, M. P. A. Fisher, A. Garg, and W. Zwerger, *Rev. Mod. Phys.* **59**, 1 (1987).
- [44] F. Gebbia, C. Benedetti, F. Benatti, R. Floreanini, M. Bina, and M. G. A. Paris, *Phys. Rev. A* **101**, 032112 (2020).
- [45] A. Candeloro and M. G. A. Paris, *Phys. Rev. A* **103**, 012217 (2021).
- [46] J.-B. Yuan, B. Zhang, Y.-J. Song, S.-Q. Tang, X.-W. Wang, and L.-M. Kuang, *Phys. Rev. A* **107**, 063317 (2023).
- [47] S. Marcantoni, *J. Phys.: Conf. Ser.* **841**, 012019 (2017).
- [48] M. Popovic, M. T. Mitchison, and J. Goold, *Proc. R. Soc. London A* **479**, 20230040 (2023).
- [49] G. Francica, *arXiv:2109.09135* (2021).
- [50] V. G. Morozov, S. Mathey, and G. Röpke, *Phys. Rev. A* **85**, 022101 (2012).

- [51] P. Liuzzo-Scorpo, L. A. Correa, F. A. Pollock, A. Górecka, K. Modi, and G. Adesso, *New J. Phys.* **20**, 063009 (2018).
- [52] P. Lipka-Bartosik and R. Demkowicz-Dobrzański, *J. Phys. A: Math. Theor.* **51**, 474001 (2018).
- [53] S. Deffner, J. P. Paz, and W. H. Zurek, *Phys. Rev. E* **94**, 010103(R) (2016).
- [54] Y. Guryanova, N. Friis, and M. Huber, *Quantum* **4**, 222 (2020).
- [55] M. Esposito, U. Harbola, and S. Mukamel, *Rev. Mod. Phys.* **81**, 1665 (2009).
- [56] P. Haikka, S. McEndoo, G. De Chiara, G. M. Palma, and S. Maniscalco, *Phys. Rev. A* **84**, 031602(R) (2011).
- [57] P. Haikka, S. McEndoo, G. D. Chiara, G. M. Palma, and S. Maniscalco, *Phys. Scr.* **T151**, 014060 (2012).
- [58] P. Haikka, T. H. Johnson, and S. Maniscalco, *Phys. Rev. A* **87**, 010103(R) (2013).
- [59] C. Addis, G. Brebner, P. Haikka, and S. Maniscalco, *Phys. Rev. A* **89**, 024101 (2014).
- [60] I. Henao and R. Uzdin, *Quantum* **5**, 547 (2021).
- [61] J. Rubio, J. Anders, and L. A. Correa, *Phys. Rev. Lett.* **127**, 190402 (2021).
- [62] J. Rubio, *Quantum Sci. Technol.* **8**, 015009 (2022).
- [63] C. W. Helstrom, *Quantum Detection and Estimation Theory* (Academic Press, New York, 1976).
- [64] S. L. Braunstein and C. M. Caves, *Phys. Rev. Lett.* **72**, 3439 (1994).
- [65] M. G. A. Paris, *Int. J. Quantum. Inf.* **07**, 125 (2009).
- [66] A. Smirne, A. Lemmer, M. B. Plenio, and S. F. Huelga, *Quantum Sci. Technol.* **4**, 025004 (2019).
- [67] R. Demkowicz-Dobrzański, M. Jarzyna, and J. Kołodyński, in *Progress in Optics*, edited by E. Wolf (Elsevier, Amsterdam, 2015), Vol. 60, pp. 345–435.
- [68] A. Smirne, J. Kołodyński, S. F. Huelga, and R. Demkowicz-Dobrzański, *Phys. Rev. Lett.* **116**, 120801 (2016).
- [69] J. F. Haase, A. Smirne, J. Kołodyński, R. Demkowicz-Dobrzański, and S. F. Huelga, *New J. Phys.* **20**, 053009 (2018).
- [70] P. Sekatski and M. Perarnau-Llobet, *Quantum* **6**, 869 (2022).
- [71] M. R. Jørgensen, P. P. Potts, M. G. A. Paris, and J. B. Brask, *Phys. Rev. Res.* **2**, 033394 (2020).
- [72] A. W. Chin, S. F. Huelga, and M. B. Plenio, *Phys. Rev. Lett.* **109**, 233601 (2012).
- [73] K. Macieszczak, *Phys. Rev. A* **92**, 010102(R) (2015).
- [74] L. A. Correa, M. Perarnau-Llobet, K. V. Hovhannisyán, S. Hernández-Santana, M. Mehboudi, and A. Sanpera, *Phys. Rev. A* **96**, 062103 (2017).
- [75] A. Fujiwara and H. Imai, *J. Phys. A: Math. Theor.* **41**, 255304 (2008).
- [76] R. Demkowicz-Dobrzański, J. Kołodyński, and M. Guţă, *Nat. Commun.* **3**, 1063 (2012).
- [77] M. Perarnau-Llobet, D. Malz, and J. I. Cirac, *Quantum* **5**, 446 (2021).
- [78] M. A. Taylor and W. P. Bowen, *Phys. Rep.* **615**, 1 (2016).
- [79] P. P. Hofer, J. B. Brask, M. Perarnau-Llobet, and N. Brunner, *Phys. Rev. Lett.* **119**, 090603 (2017).
- [80] I. Henao, K. V. Hovhannisyán, and R. Uzdin, *arXiv:2108.10469* (2021).
- [81] N. V. Gnezdilov, A. I. Pavlov, V. Ohanesjan, Y. Cheipesh, and K. Schalm, *Phys. Rev. A* **107**, L031301 (2023).
- [82] G. M. Palma, K.-A. Suominen, and A. K. Ekert, *Proc. R. Soc. London A* **452**, 567 (1996).
- [83] M. T. Mitchison, A. Purkayastha, M. Brenes, A. Silva, and J. Goold, *Phys. Rev. A* **105**, L030201 (2022).
- [84] L. Seveso and M. G. A. Paris, *Phys. Rev. A* **97**, 032129 (2018).
- [85] D. Burgarth, V. Giovannetti, A. N. Kato, and K. Yuasa, *New J. Phys.* **17**, 113055 (2015).
- [86] A. De Pasquale, K. Yuasa, and V. Giovannetti, *Phys. Rev. A* **96**, 012316 (2017).
- [87] A. Auffèves, *PRX Quantum* **3**, 020101 (2022).
- [88] S. V. Moreira, G. Adesso, L. A. Correa, T. Coudreau, A. Keller, and P. Milman, *Phys. Rev. A* **96**, 012110 (2017).
- [89] I. Antoniou, E. Karpov, G. Pronko, and E. Yarevsky, *Phys. Rev. A* **63**, 062110 (2001).
- [90] K. Bradler, P. Hayden, D. Touchette, and M. M. Wilde, *Phys. Rev. A* **81**, 062312 (2010).
- [91] S. I. Knysh and G. A. Durkin, *arXiv:1307.0470* (2013).